View metadata, citation and similar papers at core.ac.uk
brought to you by CORE
provided by Digital.CSIC

PHYSICAL REVIEW C **81**, 054305 (2010)

γ-ray spectroscopy of neutron-rich ^{40}S

Z. M. Wang,[1,*] R. Chapman,[1] X. Liang,[1] F. Haas,[2] F. Azaiez,[3] B. R. Behera,[4] M. Burns,[1] E. Caurier,[2] L. Corradi,[4] D. Curien,[2] A. N. Deacon,[5] Zs. Dombrádi,[6] E. Farnea,[7] E. Fioretto,[4] A. Gadea,[4] A. Hodsdon,[1] F. Ibrahim,[3] A. Jungclaus,[8] K. Keyes,[1] V. Kumar,[1] A. Latina,[4] S. Lunardi,[7] N. Mărginean,[4,9] G. Montagnoli,[7] D. R. Napoli,[4] F. Nowacki,[2] J. Ollier,[1,10] D. O'Donnell,[1,10] A. Papenberg,[1] G. Pollarolo,[11] M.-D. Salsac,[12] F. Scarlassara,[7] J. F. Smith,[1] K. M. Spohr,[1] M. Stanoiu,[9] A. M. Stefanini,[4] S. Szilner,[4,13] M. Trotta,[4] and D. Verney[3]

[1]*School of Engineering, University of the West of Scotland, Paisley, PA1 2BE, United Kingdom and the Scottish Universities Physics Alliance (SUPA)*
[2]*IPHC, CNRS-IN2P3 and Université de Strasbourg, F-67037 Strasbourg Cedex 2, France*
[3]*IPN, CNRS-IN2P3 and Université Paris-Sud, F-91406 Orsay Cedex, France*
[4]*INFN, Laboratori Nazionali di Legnaro, I-35020 Legnaro, Padova, Italy*
[5]*Schuster Laboratory, University of Manchester, Manchester, M13 9PL, United Kingdom*
[6]*ATOMKI, P. O. Box 51, H-4001 Debrecen, Hungary*
[7]*INFN-Sezione di Padova and Dipartimento di Fisica, Università di Padova, I-35131 Padova, Italy*
[8]*Instituto de Estructura de la Materia, CSIC, E-28006 Madrid, Spain*
[9]*Horia Hulubei National Institute of Physics and Nuclear Engineering, Strasse Atomistilor 407, P. O. Box MG-6, Bucharest, Romania*
[10]*STFC Daresbury Laboratory, Warrington, WA4 4AD, United Kingdom*
[11]*Dipartimento di Fisica Teorica, Università di Torino and INFN-Sezione di Torino, Via P. Giuria 1, I-10125 Torino, Italy*
[12]*CEA-Saclay, Service de Physique Nucléaire, F-91191 Gif-sur-Yvette Cedex, France*
[13]*Ruđer Bošković Institute, Zagreb, Croatia*

(Received 21 December 2009; revised manuscript received 12 February 2010; published 12 May 2010)

Yrast states up to (6^+) in the neutron-rich ^{40}S nucleus have been studied using binary grazing reactions produced by the interaction of a 215 MeV beam of ^{36}S ions with a thin ^{208}Pb target. The novel experimental setup that combines the large acceptance magnetic spectrometer, PRISMA, and the high-efficiency γ-ray detection array, CLARA, was used. A new γ-ray transition at an energy of 1572 keV was observed and tentatively assigned to the $(6^+) \rightarrow (4^+)$ transition. A comparison of experimental observations and the results of large-scale $0\hbar\omega$ *sd-pf* shell-model calculations indicates that one- and two-proton excitations from the $2s_{1/2}$ to the $1d_{3/2}$ orbitals play an important role in reproducing the ^{40}S yrast level structure and the published $B(E2; 0^+_{\text{g.s.}} \rightarrow 2^+_1)$ value. The structure of the yrast states of the even-A isotopes of sulfur is interpreted in terms of the configurations of valence protons and neutrons within the context of large-scale $0\hbar\omega$ *sd-pf* shell-model calculations.

DOI: 10.1103/PhysRevC.81.054305 PACS number(s): 23.20.Lv, 25.70.Lm, 27.40.+z

I. INTRODUCTION

In the atomic nucleus, the large shell gap in the energy spectrum of single-particle states is the origin of magic numbers. The traditional shell gaps can be reproduced using a single-particle harmonic oscillator potential with a strong spin-orbit interaction first suggested independently by Haxel *et al.* [1] and Mayer [2]. The magic number is the most fundamental quantity governing nuclear structure. However, single-particle energies change with increasing neutron excess, leading to the disappearance of some conventional magic numbers and the appearance of new shell gaps [3]. In the case of $^{32}_{12}$Mg$_{20}$, the unexpectedly large $B(E2; 0^+_{\text{g.s.}} \rightarrow 2^+_1)$ value [4–6] and small 2^+_1 energy [7] imply the erosion of the $N = 20$ shell gap, which has been interpreted in terms of a two particle-two hole intruder configuration that dominates the ground state (g.s.) of ^{32}Mg [8–10], leading to its intrinsic deformation.

The behavior of two-neutron separation energies as a function of neutron number for the heavy sulfur ($Z = 16$) isotopes near $N = 28$ is quite different from that for the neutron-rich potassium ($Z = 19$) and calcium ($Z = 20$) isotopes and indicates shell quenching at $N = 28$ for sulfur isotopes [11]. Experimental measurements of excitation energies and $B(E2; 0^+_{\text{g.s.}} \rightarrow 2^+_1)$ values for the first 2^+ states of neutron-rich even-A sulfur isotopes populated using intermediate-energy Coulomb excitation [12,13] indicate that the neutron-rich sulfur isotopes with $A = 40$ and 42 are deformed with $\beta_2 \sim 0.3$, in agreement with theoretical calculations by Werner *et al.* [14] and provide evidence that the $N = 28$ shell closure is somewhat eroded. The results of in-beam γ-ray spectroscopy studies of ^{40,42,44}S using fragmentation reactions at GANIL, when compared with the results of microscopic collective-model and large-scale shell-model calculations [15–17], suggest that ^{40}S and ^{42}S are deformed, γ-soft nuclei, whereas in ^{44}S, evidence has been presented for shape coexistence in the spectrum of low-energy states [18].

Excited states of ^{40}S have previously been studied in ^{40}P β decay [19], in in-beam γ-ray spectroscopy using

*zhimin.wang@uws.ac.uk

 ©2010 The American Physical Society

fragmentation reactions [15–17], in elastic and inelastic proton scattering in inverse kinematics [20], and in intermediate-energy Coulomb excitation [12,13]. For the first 2^+ state of ^{40}S, the $B(E2; 2_1^+ \rightarrow 0^+_{\text{g.s.}})$ value has been measured as $66.8 \pm 7.2\, e^2$ fm^4 by Scheit *et al.* [12]. The tentative assignment of $J^\pi = 4^+$ to a state at 1917 keV in the ^{40}P β-decay work of Winger *et al.* [19], based mainly on nuclear structure arguments, appears to be inconsistent with the fragmentation work of Sohler *et al.* [15]. Sohler has suggested an alternative level scheme to that proposed by Winger *et al.*, in which the $J^\pi = (4^+)$ level at 1917 keV is replaced by a state at 3712 keV. The level scheme from the published β-decay work of Winger *et al.*, presented later, reflects this proposed change. The second discrepancy between these two studies relates to the proposed J^π value for the state at 2265 keV. The $J^\pi = (4^+)$ assignment of Sohler *et al.* for this state is based on γ-ray anisotropy measurements and on the favored population of yrast states in fragmentation reactions, and is also supported by the absence of a γ-ray decay branch to the ^{40}S ground state. Winger *et al.* [19] proposed a $J^\pi = (2^+)$ assignment for this state.

For a more complete understanding of the structure of ^{40}S, additional experimental data are needed on relatively high-lying yrast states and especially the yrast decay sequence, $J^\pi = 0^+$, 2^+, 4^+, 6^+, and 8^+, with configurations, in a simple shell-model picture, based on the four extra-core $1f_{7/2}$ neutrons. Here the yrast decay sequence of neutron-rich ^{40}S, populated in binary grazing reactions, has been studied. We have exploited the setup that combines a large-acceptance magnetic spectrometer, PRISMA [21], and a high-granularity and high-efficiency γ-ray detection array, CLARA [22], which allows precise Doppler correction of γ-ray energy spectra and good reaction channel selection.

II. EXPERIMENT

Yrast states of the midshell, $N = 24$, nucleus ^{40}S were populated using binary grazing reactions produced in the interaction of a 215 MeV beam of $^{36}S^{9+}$ ions, delivered by the XTU-Tandem Van de Graaff-ALPI, superconducting linear accelerator, complex at the INFN Legnaro National Laboratory, Italy, with a thin ^{208}Pb target. The target, isotopically enriched to 99.7% in ^{208}Pb, was of thickness 300 μg cm^{-2} on a 20 μg cm^{-2} carbon backing. Projectile-like fragments produced during the reaction were analyzed with PRISMA, a large acceptance-angle magnetic spectrometer ($\pm 5.5^\circ$ in the dispersion plane and $\pm 10.5^\circ$ perpendicular to the dispersion plane, $\sim$80 msr solid angle), placed at 56° to the beam axis and covering a range of angles, including the grazing angle of the reaction (58°). The PRISMA spectrometer consists of a quadrupole singlet and a dipole magnet separated by 60 cm. The (x, y) coordinates and time information of an ion entering the spectrometer are measured using a position-sensitive microchannel plate (MCP) detector [23] placed at 25 cm from the target. Following the passage of each ion through the magnetic elements, the coordinates of the trajectory and time information are measured again at the focal plane of the spectrometer using a 10-element 100 cm long multiwire parallel-plate avalanche counter (MWPPAC) [24]. The position resolution of the MCP and MWPPAC is 1 mm in the horizontal (dispersive) direction, and the time resolution of the MCP and MWPPAC combination is about 300 ps. Finally, the ions are stopped in a 10×4 element ionization chamber (IC) used for energy loss, ΔE, and total energy, E, measurement [23,24]. For each ion detected in PRISMA, the preceding measurements enable us to determine the atomic number Z, the mass number A, the ion charge state, and the time of flight, thereby allowing an unambiguous identification of each detected projectile-like nucleus. Reconstruction of the trajectory of each ion through the spectrometer together with the time-of-flight measurement was used to establish the velocity vector of each ion on an event-by-event basis.

The γ rays from the deexcitation of the binary reaction products were detected using CLARA, an array of 25 escape-suppressed Ge clover detectors (22 Ge clover detectors were used during this work). The γ rays were detected in time coincidence with projectile-like fragments identified at the focal plane of the PRISMA spectrometer, thereby providing an unambiguous association of γ rays with each projectile-like binary fragment of a particular A and Z. CLARA was positioned in the hemisphere opposite to the PRISMA spectrometer and covering the azimuthal angles from 98° to 180° with respect to the entrance aperture of PRISMA. The CLARA total photopeak efficiency for 1.3 MeV γ rays is around 2.8%, and the peak-to-total ratio is 45% for ^{60}Co 1.3 MeV γ rays. Doppler correction of γ-ray energies was performed on an event-by-event basis. The energy resolution of the γ-ray photopeaks following Doppler correction was typically around 0.6%. Experimental data were accumulated during a 6 day run with an average beam current of 60 e nA.

III. RESULTS AND DISCUSSION

In this experiment, a wide range of nuclear species, from Na ($Z = 11$) to Mn ($Z = 25$), was identified at the focal plane of PRISMA. Here we will focus on a discussion of the heavy sulfur isotope ^{40}S. The mass spectrum of sulfur isotopes with mass resolution $\sim 1/140$ is presented in Fig. 1. The structures between the mass peaks originate from electronic timing problems. Careful gating of the mass spectrum was therefore essential to eliminate the possibility of contamination of the γ-ray spectrum. Figure 2 presents three one-dimensional γ-ray spectra corresponding to gates on the three indicated regions of the mass spectrum of Fig. 1. The 1517 keV photopeak, corresponding to the most intense transition observed in ^{39}S in the present work, is present in the γ-ray spectra associated with gates centered on $A = 39$ and centered between the mass 39 and 40 peaks but is absent in the spectrum corresponding to a narrow gate on ^{40}S. The γ-ray transitions from the much more intensely populated ^{39}S nucleus do not, therefore, contribute in any significant way to the spectrum corresponding to a narrow mass gate on ^{40}S. The γ-ray spectrum corresponding to a gate set around ^{41}S in the mass spectrum of Fig. 1 has two very weak photopeaks at energies of 449 and 638 keV. The 449 keV γ-ray transition was previously identified by Ibbotson *et al.* [25].

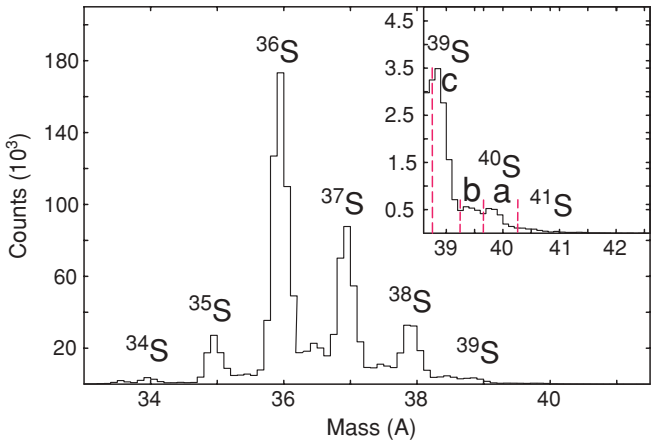

FIG. 1. (Color online) Mass spectrum for sulfur ($Z = 16$) isotopes populated in this article. See text for details.

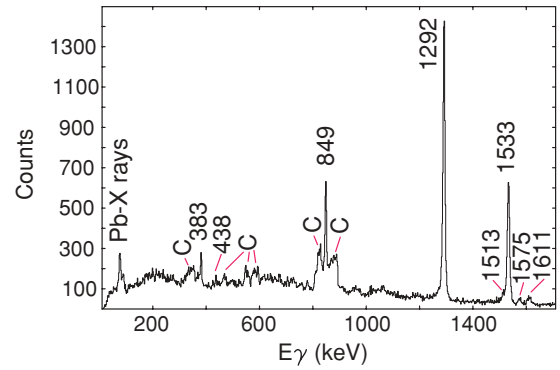

FIG. 3. (Color online) The partial γ-ray spectrum from the decay of excited states of ^{38}S populated in this article. Peaks labeled "C" correspond to the decay of targetlike fragments. The spectrum illustrates the population of yrast states in binary grazing reactions.

In the Doppler-corrected one-dimensional γ-ray spectrum from the deexcitation of excited states of ^{40}S, presented in Fig. 2(a), photopeaks at energies of 904, 1352, and 1572 keV are clearly visible; the uncertainty in γ-ray energy is approximately ± 1 keV. The photopeaks at energies of 904 and 1352 keV correspond to the previously observed $2^+ \rightarrow 0^+$ and $(4^+) \rightarrow 2^+$ transitions [15–17], respectively. To illustrate the population characteristics of binary grazing reactions, the γ-ray spectrum corresponding to the deexcitation of states in ^{38}S, also populated in this work, is presented in Fig. 3. Transitions within the known ^{38}S yrast decay sequence of 1292, 1533, and 849 keV, corresponding to the $2^+ \rightarrow 0^+$, $4^+ \rightarrow 2^+$, and $(6^+) \rightarrow 4^+$ γ-ray transitions [26–28], respectively, correspond to the most intense photopeaks observed in the spectrum of Fig. 3. In the spectrum of Fig. 2, the photopeak at an energy of 1572 keV corresponds to a γ-ray transition previously unknown in the decay sequence of ^{40}S. On the basis of the population characteristics of binary grazing reactions, together with a consideration of relative transition intensities, the 1572 keV γ-ray photopeak is tentatively assigned to the yrast $(6^+) \rightarrow (4^+)$ transition of ^{40}S.

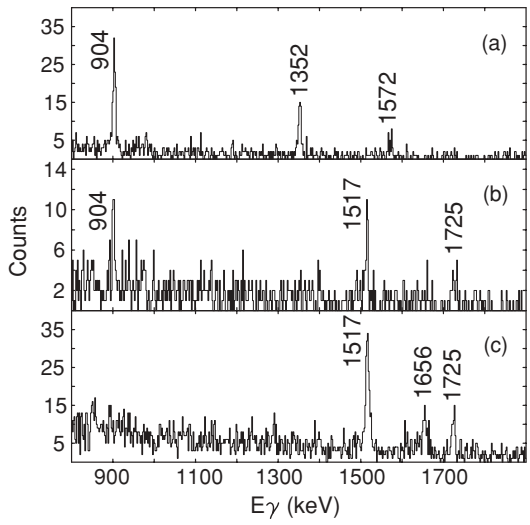

FIG. 2. Doppler-corrected partial γ-ray spectra corresponding to gates set in regions a to c of the mass spectrum of Fig. 1. (top) Spectrum corresponds to region a of the mass spectrum and shows γ-ray transitions within the ^{40}S yrast decay sequence. (bottom) Spectrum dominated by yrast transitions in ^{39}S. (middle) Spectrum corresponds to a gate set between the mass 39 and 40 peaks of Fig. 1. See text for details.

The midshell $^{40}_{16}S_{24}$ nucleus has four neutrons outside the $N = 20$ major shell occupying the $1f_{7/2}$ orbital, leading to states with J^π values of 0^+, 2^+, 4^+, 6^+, and 8^+. For these $\upsilon(1f_{7/2})^4$ yrast states, we would expect, in a simple shell-model picture, protons to fill the $1d_{5/2}$ and $2s_{1/2}$ single-particle states. To obtain a more informed microscopic description of the present experimental results, we have performed large-scale $0\hbar\omega$ *sd-pf* shell-model calculations for ^{40}S using the ANTOINE code [29,30]. The new SDPF-U effective interaction [31] was employed. In the first calculation, an *sd-pf* model space was used, in which protons are allowed to move within the full *sd* shell and the four extra-core neutrons are free to occupy full *pf* orbitals, the normal configuration space for the SDPF-U interaction. In such a calculation, only positive-parity states can be obtained, of course. In the following discussion, we refer to this calculation as SM1. A comparison of the experimental yrast level energies and the published experimental $B(E2)$ value [12] with the results of the $0\hbar\omega$ *sd-pf* shell-model calculation is presented in Fig. 4 and Table I. Only the first three states of each J^π value are presented in Fig. 4. The calculation is able to reproduce the experimental data in a satisfactory way. Table II presents the main components ($\geqslant 10\%$) of the shell-model wave functions of the ^{40}S yrast states. From Table II it can be seen that the occupation of the $1d_{3/2}$ orbital by protons in the states considered here is significant, accounting for between 20% and 40% of the wave function. The occupation of the $1f_{5/2}$ and $2p$ orbitals by neutrons accounts for, typically, less than 10% of the wave function.

To investigate the influence of the occupation of the $1d_{3/2}$ orbital by protons and the occupation of the $1f_{5/2}$ and $2p$ orbitals by neutrons, we have performed two further calculations, identical to the SM1 calculation, but in which

TABLE I. Comparison of level energies from this article and $B(E2)$ values taken from Ref. [12] with the results of shell-model calculations for the ^{40}S nucleus. See text for details.

J^π	E_x(keV)			
	Exp.	SM1	SM2	SM3
0^+	0	0	0	0
2^+	904	942	1138	1355
4^+	2256	2173	2199	2265
6^+	3828	3651	3105	3160
$J_i^\pi \to J_f^\pi$	$B(E2; J_i \to J_f)$ (e^2 fm^4)			
	Exp.	SM1	SM2	SM3
$2^+ \to 0^+$	66.8 ± 7.2	78	60	13
$4^+ \to 2^+$		93	58	12
$6^+ \to 4^+$		77	59	6

these orbitals were blocked. In the first of these calculations, SM2, neutrons were confined to the $1f_{7/2}$ shell and protons were free to occupy the full *sd* shell. In the second calculation, SM3, protons were confined to the $1d_{5/2}$ and $2s_{1/2}$ orbitals, and neutrons were free to move within the full *pf* shell. A comparison of the experimental yrast level energies and the published experimental $B(E2)$ value [12] with the results of the two additional shell-model calculations is also presented in Fig. 4 and Table I. In the calculation of $B(E2)$ values, effective charges of $0.5e$ for neutrons and $1.5e$ for protons were used. The calculation SM1, as we expect, provides the best overall comparison with the experimental yrast energies and the $B(E2)$ value. A comparison of the results of calculations SM1 and SM2 with experiment highlights the important role that neutron excitations into the $1f_{5/2}$ and $2p$ orbitals play, especially in reproducing level energies, although the amplitudes of such configurations in the calculation SM1 are, as we have noted earlier, smaller than 10% (see Table II). The poorest agreement with experiment, particularly in relation to the $B(E2; 2_1^+ \to 0^+_{\text{g.s.}})$ value, corresponds to the calculation SM3, in which protons are confined to the $1d_{5/2}$ and $2s_{1/2}$ shell-model orbitals. It may therefore be concluded that within the model space employed here, the wave functions of the yrast states have important proton $\pi(2s_{1/2})^1(1d_{3/2})^1$ and $\pi(2s_{1/2})^0(1d_{3/2})^2$ components, which, taken together, account for about 20%–40% of the wave function (see Table II).

The level lifetime of the first 2^+ state deduced from the SM1 shell-model $B(E2)$ value, and using the experimental value of the $2_1^+ \to 0^+_{\text{g.s.}}$ transition energy, is 17.3 ps, which is comparable to the experimental value of 21.1 ± 3.4 ps [12,32]. The level lifetimes deduced from the SM1 shell-model calculations for the 4^+ and 6^+ states are 1.9 and 1.1 ps, respectively. The lifetimes are consistent with the nonobservation of the $4^+ \to 2^+$ and $6^+ \to 4^+$ yrast transitions in earlier thick-target experiments [26–28] in which ^{40}S was populated in deep-inelastic collision processes. The slowing-down time of projectile-like nuclear species in the thick target is of the order of 1 ps.

TABLE II. Main components of the wave functions of the yrast states of ^{40}S from the SM1, SM2, and SM3 shell-model calculations. See text for details.

J^π	E_x (keV)	Main components of wave function	Percentage ($\geqslant$10%)
		SM1	
0^+	0	$\pi(2s_{1/2})^2 \otimes \upsilon(1f_{7/2})^4$	18
		$\pi(1d_{3/2})^2 \otimes \upsilon(1f_{7/2})^4$	22
2^+	942	$\pi(2s_{1/2})^1(1d_{3/2})^1 \otimes \upsilon(1f_{7/2})^4$	16
		$\pi(1d_{3/2})^2 \otimes \upsilon(1f_{7/2})^4$	18
4^+	2173	$\pi(2s_{1/2})^2 \otimes \upsilon(1f_{7/2})^4$	11
		$\pi(2s_{1/2})^1(1d_{3/2})^1 \otimes \upsilon(1f_{7/2})^4$	15
		$\pi(1d_{3/2})^2 \otimes \upsilon(1f_{7/2})^4$	19
6^+	3651	$\pi(2s_{1/2})^2 \otimes \upsilon(1f_{7/2})^4$	16
		$\pi(2s_{1/2})^1(1d_{3/2})^1 \otimes \upsilon(1f_{7/2})^4$	16
		$\pi(1d_{3/2})^2 \otimes \upsilon(1f_{7/2})^4$	22
		SM2	
0^+	0	$\pi(2s_{1/2})^2$	30
		$\pi(2s_{1/2})^1(1d_{3/2})^1$	13
		$\pi(1d_{3/2})^2$	33
2^+	1138	$\pi(2s_{1/2})^2$	19
		$\pi(2s_{1/2})^1(1d_{3/2})^1$	26
		$\pi(1d_{3/2})^2$	32
4^+	2199	$\pi(2s_{1/2})^2$	22
		$\pi(2s_{1/2})^1(1d_{3/2})^1$	24
		$\pi(1d_{3/2})^2$	33
6^+	3105	$\pi(2s_{1/2})^2$	26
		$\pi(2s_{1/2})^1(1d_{3/2})^1$	21
		$\pi(1d_{3/2})^2$	31
		SM3	
0^+	0	$\upsilon(1f_{7/2})^4$	70
		$\upsilon(1f_{7/2})^2(2p_{3/2})^2$	15
2^+	1355	$(1f_{7/2})^4$	62
		$\upsilon(1f_{7/2})^3(2p_{3/2})^1$	18
4^+	2265	$\upsilon(1f_{7/2})^4$	65
		$\upsilon(1f_{7/2})^3(2p_{3/2})^1$	24
6^+	3160	$\upsilon(1f_{7/2})^4$	85

We now discuss the structure of ^{40}S within the context of the evolving structure of the isotopes of the neutron-rich sulfur isotopes. With increasing neutron number, between $N = 22$ and 28, the energy spacing of the proton $2s_{1/2}$ and $1d_{3/2}$ orbitals decreases and the $3/2^+$ and $1/2^+$ states eventually cross over. The first experimental observation of the $2s_{1/2}$-$1d_{3/2}$ inversion was made by Bjerregaard *et al.* [33] in 1967; in this work, states of ^{47}K were populated in the proton pickup reaction (t, α). From more recent studies of proton pickup reactions on the even-A isotopes of calcium, the evolution of the $d_{3/2}$ and $s_{1/2}$ proton-hole states in the potassium isotopes has been established for $20 \leqslant N \leqslant 28$ [34,35]. The monopole component of the tensor interaction between neutrons in the

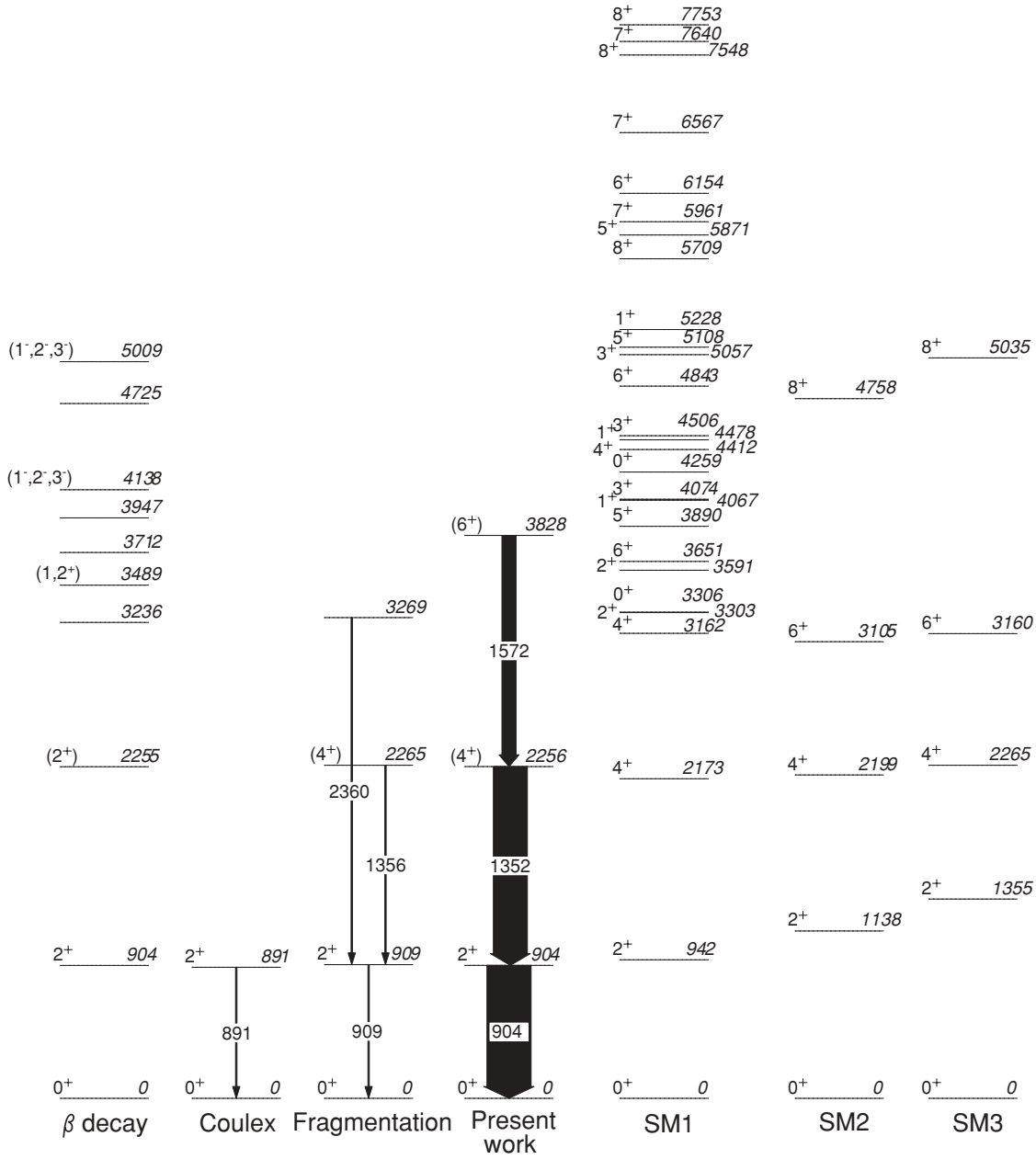

FIG. 4. Comparison of the present experimental level scheme for ^{40}S with the previous experimental results [12,13,15–17,19,20] and the results of large-scale $0\hbar\omega$ *sd-pf* shell-model calculations. Only yrast states are shown for calculations SM2 and SM3. See text for details. The arrow widths of the γ transitions in the ^{40}S level scheme from this article are proportional to the measured relative γ-ray intensities.

$1f_{7/2}$ shell and protons in the $1d_{3/2}$ shell is responsible for the increase in binding of protons in the $1d_{3/2}$ orbit as neutrons fill the $1f_{7/2}$ shell. For the isotopes of potassium, the total monopole shift between $1d_{3/2}$ and $2s_{1/2}$ proton binding is about 350 keV per $1f_{7/2}$ neutron [36]. This behavior has also been observed in the phosphorus [37] and chlorine [38] isotopes, but here the behavior of the energy splitting as a function of neutron number is different, in detail, from that for the isotopes of potassium. The significance of the near-degeneracy of the $\pi(1d_{3/2})$ and $\pi(2s_{1/2})$ orbitals with increasing neutron number is that this results in a deformation-driving force related to the pseudo-SU(3) symmetry of the two orbits [39]. This is the underlying reason for the onset of deformation in neutron-rich sulfur isotopes with increasing neutron number [12,40]. In addition, as neutrons are added to the $1f_{7/2}$ shell, there will be a tendency for the nucleus to acquire a quadrupole deformation to remove the degeneracy of the $1f_{7/2}$ orbit; this is the nuclear analog of the Jahn-Teller effect [41,42]. The quadrupole deformation in the neutron-rich isotopes of sulfur reaches a maximum at ^{42}S [13] and $N = 28$ ^{44}S has an appreciable value of β_2, the quadrupole deformation parameter.

The evolving structure of the sulfur isotopes for $22 \leqslant N \leqslant 28$ is now discussed within the context of the shell model in which the new effective interaction for $0\hbar\omega$ calculations in the *sd-pf* valence space is used. Figure 5 presents the first 2^+ energies and $B(E2; 2_1^+ \rightarrow 0^+_{\text{g.s.}})$ values for the even-A

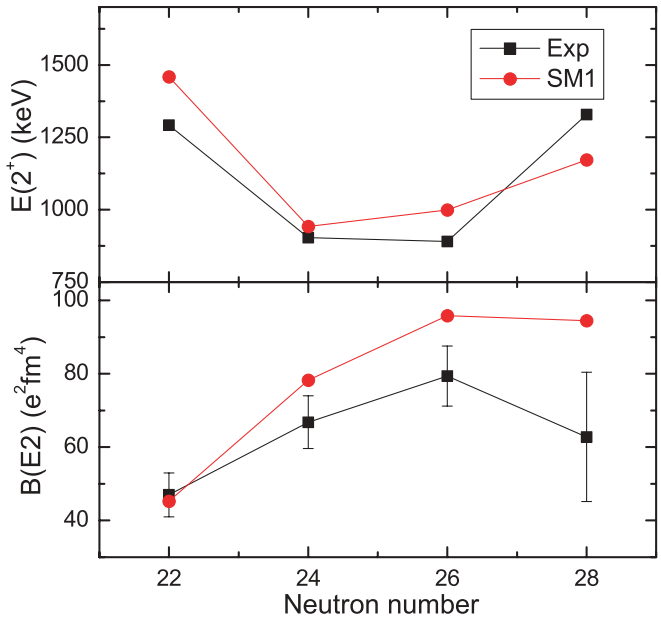

FIG. 5. (Color online) The systematics of experimental 2_1^+ energies and $B(E2;2_1^+ \rightarrow 0_{g.s.}^+)$ values in even-A sulfur isotopes for neutron numbers in the range $22 \leqslant N \leqslant 28$.

isotopes of sulfur for neutron numbers in the range 22–28. The first 2^+ energies of ^{38}S, ^{40,42}S, and ^{44}S were taken from Refs. [12,13,43], respectively. The $B(E2;2_1^+ \rightarrow 0_{g.s.}^+)$ values for ^{38,40,42}S and ^{44}S were taken from Refs. [12,13], respectively. The 2_1^+ energies reach a minimum and the $B(E2;2_1^+ \rightarrow 0_{g.s.}^+)$ values a maximum at $N = 26$. For the $N = 28$ isotope, ^{44}S, the $B(E2;2_1^+ \rightarrow 0_{g.s.}^+)$ value is a factor 3.3 larger and the 2_1^+ energy, 1297 keV, is significantly smaller than for the $N = 20$ closed-shell nucleus, ^{36}S. The available evidence suggests that the $N = 28$ shell gap at $Z = 16$ is somewhat quenched. The shell-model calculation provides good overall agreement with the experimental 2_1^+ energies and the experimental $B(E2;2_1^+ \rightarrow 0_{g.s.}^+)$ values (see Fig. 5). The wave functions presented in Table III illustrate the importance

TABLE III. Total percentage of $\pi(2s_{1/2})^1(1d_{3/2})^1$ and $\pi(2s_{1/2})^0(1d_{3/2})^2$ components in the wave functions of the $0_{g.s.}^+$ and 2_1^+ states of the even-A sulfur isotopes for neutron numbers in the range $22 \leqslant N \leqslant 28$. Only configurations involving proton excitations from the $2s_{1/2}$ to the $1d_{3/2}$ orbitals are included.

^xS	J^π	$\pi(2s_{1/2})^1(1d_{3/2})^1$ (%)	$\pi(2s_{1/2})^0(1d_{3/2})^2$ (%)
^{38}S	$0_{g.s.}^+$	11	15
	2_1^+	28	17
^{40}S	$0_{g.s.}^+$	20	31
	2_1^+	27	29
^{42}S	$0_{g.s.}^+$	19	36
	2_1^+	25	31
^{44}S	$0_{g.s.}^+$	9	39
	2_1^+	18	30

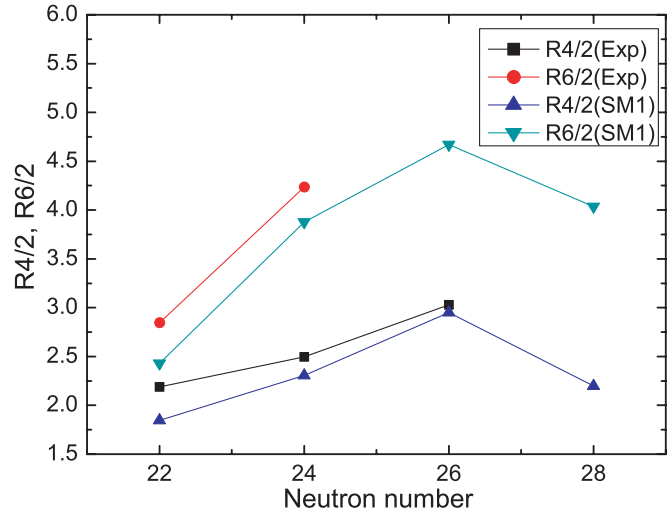

FIG. 6. (Color online) Systematics of the $E(4^+)/E(2^+)$ and $E(6^+)/E(2^+)$ ratios for sulfur isotopes with neutron numbers from $N = 22$ to 28. The $E(6^+)/E(2^+)$ datum point for $N = 24$ is based on this work.

of the $\pi(2s_{1/2})^1(1d_{3/2})^1$ and $\pi(2s_{1/2})^0(1d_{3/2})^2$ configurations in the description of the $0_{g.s.}^+$ and 2_1^+ states of the even-A neutron-rich isotopes of sulfur. With the exception of the ground state of ^{38}S, proton excitations into the $1d_{3/2}$ orbital account for approximately 50% of the wave function of the $0_{g.s.}^+$ and first 2^+ states.

The experimental $R4/2 = E(4^+)/E(2^+)$ ratios for the even-A sulfur isotopes with neutron numbers in the range of $22 \leqslant N \leqslant 26$ are presented in Fig. 6. For ^{38}S and ^{40,42}S, the data were taken from Ref. [43] and Refs. [15–17], respectively. For the heaviest sulfur isotope for which such data are available, ^{42}S, the ratio is within 10% of that corresponding to a rigid rotor. A quadrupole deformation parameter, β_2, of magnitude 0.300(24) was obtained for ^{42}S by Scheit *et al.* [12] from the measurement of $B(E2;0_{g.s.}^+ \rightarrow 2_1^+)$. The available $R6/2 = E(6^+)/E(2^+)$ ratios for the even-A sulfur isotopes are also presented in Fig. 6. The energy of the $J^\pi = (6^+)$ state of ^{38}S was taken from Ref. [26], and for ^{40}S, the value comes from this work. As may be seen from Fig. 6, there is good overall agreement between experiment and the results of the shell-model calculations. There is currently no experimental information about the location of the yrast 4^+ and 6^+ states of ^{44}S. In the shell-model calculations performed here (SM1), these states are predicted at excitation energies of 2575 and 4728 keV, respectively.

IV. CONCLUSIONS

The yrast decay sequence of ^{40}S has been observed for the first time up to the (6^+) state. The experimental yrast level energies and $B(E2)$ value are in excellent agreement with the results of $0\hbar\omega$ full *sd-pf* model-space shell-model calculations using the ANTOINE code with the SDPF-U interaction. The calculations also show that $\pi(2s_{1/2})^1(1d_{3/2})^1$ and $\pi(2s_{1/2})^0(1d_{3/2})^2$ configurations play an important role in a

description of the observed yrast states and $B(E2)$ values not only for ^{40}S but also for the even-A isotopes of sulfur with $22 \leqslant N \leqslant 28$. The available $E(4^+)/E(2^+)$ and $E(6^+)/E(2^+)$ ratios for the even-A sulfur isotopes are also well reproduced by the current shell-model calculations.

ACKNOWLEDGMENTS

This work was supported in part by the EPSRC (UK) and by the European Union under Contract No. RII3-CT-2004-506065. Five of us (D.O., M.B., A.H., K.K., and A.P.) acknowledge financial support from the EPSRC. A.N.D. acknowledges support from STFC. Z.M.W. acknowledges support from ORSAS and from the University of the West of Scotland. A.J. acknowledges financial support from the Spanish Ministerio de Ciencia e Innovación under Contract Nos. FPA2007-66069 and FPA2009-13377-C02-02. Zs.D. acknowledges financial support from OTKA Project No. K68801. The contribution of the accelerator and target-fabrication staff at the INFN Legnaro National Laboratory is gratefully acknowledged.

[1] O. Haxel, J. H. Jensen, and H. E. Suess, Phys. Rev. **75**, 1766 (1949).
[2] M. G. Mayer, Phys. Rev. **75**, 1969 (1949).
[3] T. Otsuka, R. Fujimoto, Y. Utsuno, B. A. Brown, M. Honma, and T. Mizusaki, Phys. Rev. Lett. **87**, 082502 (2001).
[4] T. Motobayashi *et al.*, Phys. Lett. B **346**, 9 (1995).
[5] B. V. Pritychenko *et al.*, Phys. Lett. B **461**, 322 (1999).
[6] V. Chiste *et al.*, Phys. Lett. B **514**, 233 (2001).
[7] C. Détraz, D. Guillemaud, G. Huber, R. Klapisch, M. Langevin, F. Naulin, C. Thibault, L. C. Carraz, and F. Touchard, Phys. Rev. C **19**, 164 (1979).
[8] A. Poves and J. Retamosa, Phys. Lett. B **184**, 311 (1987).
[9] A. Poves and J. Retamosa, Nucl. Phys. A **571**, 221 (1994).
[10] A. Watt, R. P. Singhal, M. H. Storm, and R. R. Whitehead, J. Phys. G **7**, L145 (1981).
[11] F. Sarazin *et al.*, Phys. Rev. Lett. **84**, 5062 (2000).
[12] H. Scheit *et al.*, Phys. Rev. Lett. **77**, 3967 (1996).
[13] T. Glasmacher *et al.*, Phys. Lett. B **395**, 163 (1997).
[14] T. R. Werner, J. A. Sheikh, M. Misu, W. Nazarewicz, J. Rikovska, K. Heeger, A. S. Umar, and M. R. Strayer, Nucl. Phys. A **597**, 327 (1996).
[15] D. Sohler *et al.*, Phys. Rev. C **66**, 054302 (2002).
[16] F. Azaiez, Nucl. Phys. A **704**, 37c (2002).
[17] D. Guillemaud-Mueller, Eur. Phys. J. A **13**, 63 (2002).
[18] S. Grevy *et al.*, Eur. Phys. J. A **25**, 111 (2005).
[19] J. A. Winger, P. F. Mantica, R. M. Ronningen, and M. A. Caprio, Phys. Rev. C **64**, 064318 (2001).
[20] F. Marechal *et al.*, Phys. Rev. C **60**, 034615 (1999).
[21] A. M. Stefanini *et al.*, Nucl. Phys. A **701**, 217c (2002).
[22] A. Gadea (EUROBALL Collaboration and PRISMA-2 Collaboration), Eur. Phys. J. A **20**, 193 (2004).
[23] G. Montagnoli *et al.*, Nucl. Instrum. Methods Phys. Res. A **547**, 455 (2005).
[24] S. Beghini *et al.*, Nucl. Instrum. Methods Phys. Res. A **551**, 364 (2005).
[25] R. W. Ibbotson, T. Glasmacher, P. F. Mantica, and H. Scheit, Phys. Rev. C **59**, 642 (1999).
[26] B. Fornal *et al.*, Phys. Rev. C **49**, 2413 (1994).
[27] X. Liang, Ph.D. thesis, University of Paisley (2001).
[28] J. Ollier, Ph.D. thesis, University of Paisley (2004).
[29] E. Caurier and F. Nowacki, Acta Phys. Pol. B **30**, 705 (1999).
[30] E. Caurier, G. Martinez-Pinedo, F. Nowacki, A. Poves, and A. P. Zuker, Rev. Mod. Phys. **77**, 427 (2005).
[31] F. Nowacki and A. Poves, Phys. Rev. C **79**, 014310 (2009).
[32] [http://www.nndc.bnl.gov/ensdf].
[33] J. H. Bjerregaard, O. Hansen, O. Nathan, R. Stock, R. Chapman, and S. Hinds, Phys. Lett. B **24**, 568 (1967).
[34] P. Doll, G. J. Wagner, K. T. Knopfle, and G. Mairle, Nucl. Phys. A **263**, 210 (1976).
[35] S. M. Banks, B. M. Spicer, G. G. Shute, V. C. Officer, G. J. Wagner, W. E. Dollhopf, L. Qingli, C. W. Glover, D. W. Devins, and D. L. Friesel, Nucl. Phys. A **437**, 381 (1985).
[36] O. Sorlin and M. G. Porquet, Prog. Part. Nucl. Phys. **61**, 602 (2008).
[37] A. Gade *et al.*, Phys. Rev. C **74**, 034322 (2006).
[38] X. Liang *et al.*, Phys. Rev. C **66**, 037301 (2002).
[39] J. Retamosa, E. Caurier, F. Nowacki, and A. Poves, Phys. Rev. C **55**, 1266 (1997).
[40] E. Khan *et al.*, Nucl. Phys. A **694**, 103 (2001).
[41] P. G. Reinhard and E. W. Otten, Nucl. Phys. A **420**, 173 (1984).
[42] W. Nazarewicz, Nucl. Phys. A **574**, 27c (1994).
[43] J. W. Olness, E. K. Warburton, J. A. Becker, D. J. Decman, E. A. Henry, L. G. Mann, and L. Ussery, Phys. Rev. C **34**, 2049 (1986).